

Band structure of stage 1-3 PdAl_2Cl_8 intercalated graphite

R.T.F. van Schaijk and A. de Visser

*Van der Waals-Zeeman Institute, University of Amsterdam,
Valckenierstraat 65, 1018 XE Amsterdam, The Netherlands*

E. McRae and R. Vangelisti

*Laboratoire de Chimie du Solide Minéral, Université Henri Poincaré - Nancy 1,
U.M.R.. C.N.R.S. 7555, B.P. 239, 54506 Vandoeuvre les Nancy Cedex, France*

Abstract

The effect of staging ($n \leq 3$) on the two-dimensional (2D) Fermi surface of PdAl_2Cl_8 acceptor-type graphite intercalation compounds (GICs) has been investigated by the Shubnikov-de Haas effect. For the stage 1 and stage 2 compounds, one and two fundamental frequencies are observed, respectively. The measured angular variation of the fundamental frequencies confirms the 2D nature of the stage 1-2 compounds. The energy spectrum is adequately described by the Blinowski-Rigaux 2D band structure model. We extract values for the intraplane carbon-carbon interaction parameter γ_0 of 2.94 eV and 2.60 eV for the stage 1 and stage 2 compound, respectively. For the stage 3 compound, the Blinowski-Rigaux model no longer applies and clear deviations from the 2D behavior are found. For one of the fundamental frequencies we find that the Fermi surface is a weakly undulating cylinder. The undulation is attributed to additional interactions between the graphite subsets across the intercalant layers, with an energy parameter $t = 5.6$ meV.

PACS: 71.18.+y, 71.20.Tx, 72.15.Gd

Corresponding author: Dr. A. de Visser

Van der Waals-Zeeman Institute, University of Amsterdam
Valckenierstraat 65, 1018 XE Amsterdam, The Netherlands
Phone: +31-20-5255732
Fax: +31-20-5255788
E-mail: devisser@wins.uva.nl

I. INTRODUCTION

The staging phenomenon is an intriguing property of graphite intercalation compounds (GICs). The possibility to insert many different atoms or chemicals in between the graphite layers is the result of an intricate balance between the interlayer Van der Waals binding forces and the elastostatic energy due to the charge transfer between host and intercalate. Over the past years many different GICs have been synthesized and characterized¹⁻³. GICs show a variety of interesting materials properties, such as superconductivity, complex magnetic ground states and high conductivities combined with low specific weights. Furthermore, GICs offer interesting perspectives to study fundamental issues like charge transfer and dimensionality crossover effects.

In this paper we concentrate on a series of low stage (stage number $n \leq 3$) PdAl_2Cl_8 acceptor-type GICs. Due to charge transfer from the carbon layers to the intercalant layers, the free carriers in the carbon layers are holes. The carrier densities in PdAl_2Cl_8 GICs amount to $\sim 1 \times 10^{27} \text{ m}^{-3}$, which is a factor ~ 1000 higher than in pure graphite. Our choice of investigating PdAl_2Cl_8 GICs is motivated by the strongly anisotropic electronic parameters for the stage 1 compound reported by Polo and co-workers⁴. Notably, the anisotropy ratio in the electrical conductivity σ_a/σ_c (where σ_a is the in-plane conductivity and σ_c the conductivity along the hexagonal axis) is extremely high: $1-2 \times 10^6$ at $T = 4.2 \text{ K}$, compared to a value of 10^4 in pure graphite. This extremely high anisotropy ratio is comparable to that reported⁵ for stage 1 and 2 AsF_5 GICs and, consequently, the Fermi surface and energy spectrum should be strictly two-dimensional (2D). The possibility of preparing low stage ($n \leq 3$) PdAl_2Cl_8 GICs in a pure and quasi single-crystalline form enables us to study the energy spectrum as a function of the stage number and to investigate dimensionality crossover effects. Detailed knowledge of the electronic band structure, such as the Fermi surface, effective mass and carrier concentration, is of significant importance for understanding the unusual properties of GICs.

The aim of our work is to determine the band structure of stage 1-3 PdAl_2Cl_8 GICs by means of the Shubnikov-de Haas (SdH) effect and to analyze the results within the framework of the 2D band structure model proposed by Blinowski and co-workers⁶. In the Blinowski-Rigaux (BR) model GICs are treated as stacks of independent subsets of n graphite layers bound by intercalant layers. Using a tight-binding method, which takes only the neighboring carbon interactions within the graphite subsets into account, the energy spectrum is calculated

and the resulting Fermi surfaces are straight cylinders. Our data show that the BR model yields a proper description for the stage 1-2 PdAl_2Cl_8 compounds, however, for the stage 3 compound clear deviations from the 2D behavior appear, which we attribute to interactions across the intercalant layers.

In recent years a number of systematic studies of the Fermi surface of acceptor-type GICs have appeared in the literature^{1,2,7}. Especially noteworthy studies of the effect of staging on the band structure have been reported for stage 1-2 InCl_3 (Ref.8) and stage 1-3 SbCl_5 GICs (Ref.9). However, in these materials the intercalate layer can be ordered and commensurate with the hexagonal graphite lattice. This gives rise to zone folding which results in complicated combination orbits of the carriers in a magnetic field. This hampers the interpretation of the experimental results and a comparison with band-structure models. In the case of PdAl_2Cl_8 GIC the intercalant does not exhibit long-range order, but remains "liquid-like" and zone folding is absent.

Magnetotransport experiments have been carried out at temperatures $T=1.5$ K and 4.2 K in magnetic fields up to 38 T on good-quality quasi-single-crystalline samples. For fields $B>10$ T, pronounced Shubnikov-de Haas oscillations were observed. The paper is organised as follows. In section II we describe the experimental details, such as sample preparation and the measuring methods. In section III we present the main experimental results. Section IV deals with the analysis of the SdH data obtained on the stage 1-3 compounds within the Blinowski-Rigaux model. Finally we present the conclusions in section V.

II. SYNTHESIS OF PdAl_2Cl_8 GIC AND EXPERIMENTAL METHODS

The chloroaluminate $\text{Pd}(\text{AlCl}_4)_2$ was synthesized by heating a mixture of 1/3 PdCl_2 and 2/3 AlCl_3 (molar fractions) until obtention of a homogeneous liquid. Slow cooling led to formation of red needle-like PdAl_2Cl_8 crystals. The graphite used in these studies was highly oriented pyrographite (PGCCL-Carbon Lorraine or ZYB - Union Carbide) in the form of rectangular bars ($15 \times 2 \times 0.1$ mm³) or 4 mm diameter discs. The first stage samples are obtained by the action of PdAl_2Cl_8 vapor on graphite under an excess of chlorine gas (0.5-0.7 atm at 25 °C) using a two zone pyrex reactor placed in a two temperature furnace (300-310 °C; 4 days)¹⁰. To prepare the second or the third stage compounds, we heated (at 320 °C, under chlorine) a mixtures of graphite and chloroaluminate with gravimetric ratios deduced from the

stage 1 chemical composition $C_{22}PdAl_2Cl_{8.5}$. Stage fidelity was determined by (00l) x-ray diffraction analyses. The thickness of the intercalant layer is $d_i=9.56\pm0.02\text{\AA}$ leading to the c-axis repeat distance $I_c= d_i+(n-1)d_0$, where $d_0= 3.35\text{ \AA}$ is the c-axis lattic parameter of graphite and n is the stage number.

The samples were mounted on a rotating sample platform in order to enable angular dependent magnetotransport measurements. The angle θ between the magnetic field and the c-axis could be determined within 0.2° . Voltage and current leads were attached to the sample by silver paint under a protective nitrogen atmosphere. The transverse magnetoresistance was measured with a standard four-point dc technique for currents, $I<0.2\text{ A}$, directed in the hexagonal plane (i.e. along the long axis of the sample). High magnetic fields were produced in the 40 T long-pulse magnet of the University of Amsterdam. Shubnikov-de Haas data were obtained in the free decay mode, after ramping the field to its maximum value. The total pulse duration amounts to 1 s. Experiments were carried out at $T= 4.2\text{ K}$ and 1.5 K with the samples immersed in liquid helium in order to ensure stable temperatures.

III. EXPERIMENTAL RESULTS

The primary results of our magnetoresistance experiments on the stage 1-3 $PdAl_2Cl_8$ GICs are presented in Figs.1-3. For all three stages, we measured several samples taken from different batches. For the stage 1 and 2 compounds small differences, of the order of 1-2%, were found in certain SdH frequencies, which we attribute to small differences in carrier density due to small differences in chemical composition and charge transfer. The reproducibility of the data confirms that the SdH frequencies present the intrinsic properties of the stage 1-3 compounds. In Table I we have collected a number of relevant parameters deduced from the SdH data. The indicated frequencies were obtained by averaging over different samples.

In Fig.1 we show the magnetoresistance, $R(B)-R(B=0)$, of a stage 1 compound measured at $T= 4.2\text{ K}$. Pronounced monochromatic SdH oscillations appear for $B> 10\text{ T}$. After subtracting the background contribution, estimated by smoothly extrapolating the low-field data to higher fields, we calculated the Fourier transform which is shown in the inset. A fundamental frequency F_1 is found at 1190 T. The small peak F_2 at 2380 T is its second harmonic. From the period of the SdH oscillation, the extremal cross-section of the Fermi surface

$S = \pi(k_F)^2 = (2\pi e/\hbar)F$ and the carrier density $n_{\text{SdH}} = 4S/(2\pi)^2 I_c$ can be calculated. We find $n_{\text{SdH}} = 1.20 \times 10^{27} \text{ m}^{-3}$.

In order to determine whether the whole Fermi surface has been observed in the SdH experiment n_{SdH} may be compared with the density $n_H = 1/R_H e$, where the Hall constant $R_H = V_H d/IB$ is calculated from the low-field Hall data. Here V_H is the Hall voltage and d is the thickness of the sample. However, we did not obtain reliable values for R_H , which we attribute to the non ideal Hall voltage contacts on the sample. The contacts were made by gluing thin copper leads to the side (thickness d) of the sample by means of silver paint. Apparently, the thickness of the conducting layer is not identical to the physical thickness of the sample, as we obtained values for n_H a factor 10 lower than n_{SdH} . Despite the fact that we could not obtain proper Hall data, we are confident that our SdH data disclose the complete Fermi surface. The SdH data of the stage 1-2 compounds can be well accounted for in the Blinowski-Rigaux band structure model (see section IV).

In Fig.2 we show the experimental data for the stage 2 compound taken at $T = 4.2$ K. Non-monochromatic SdH oscillations appear for $B > 10$ T. The Fourier transform of the data is shown in the inset. We observe six frequencies, labelled F_1 - F_6 . In Fig.3 we show the magnetoresistance of the stage 3 compound measured at $T = 1.5$ K. In the inset the Fourier transform of the SdH data is shown. One strong frequency component and a number of weaker components can be observed. In section IV we offer an explanation for the observed Fourier spectra.

The angular dependence of the SdH frequencies was measured for the stage 1-3 compounds at $T = 4.2$ K. For the stage 1 and 2 GICs, we could observe the SdH effect up to an angle θ of $\sim 25^\circ$. For both stages, the fundamental frequency F_1 followed the relation $F_1(\theta) = F_1(0)/\cos\theta$, as expected for a 2D cylindrical Fermi surface. For the stage 3 compound we could follow the SdH effect up to $\sim 35^\circ$. In Fig.4 we show the SdH signals of the stage 3 compound for three different angles measured at $T = 4.2$ K. Upon increasing the angle, both the frequency and amplitude decrease. The angular variation of the strongest frequency component (peak 4 in the inset of Fig. 3) is traced in Fig.5. For a straight 2D cylindrical Fermi surface the data should follow the dashed line. Significant deviations from this behavior appear for $\theta > 15^\circ$ (the size of the symbols indicate the error bars). As we will show in section

IV.C the data follow the angular dependence of the smallest circular cross section of a weakly undulating cylindrical Fermi surface (solid line in Fig.5).

Cyclotron effective masses were determined from the temperature dependence of the amplitude of the SdH oscillation for the stage 1 and stage 3 compound. Since we have taken data only at $T=4.2$ K and 1.5 K the accuracy is limited. For the stage 1 compound the effective mass equals $m^*/m_0= 0.25\pm 0.05$ (m_0 is the free electron mass). For the stage 3 compound we only determined the effective mass for the frequency components F_2 and F_4 (see Table I).

IV. ANALYSIS AND DISCUSSION

A. Stage 1 compound

In acceptor-type GICs, strong anisotropy in the electrical conductivity is often observed¹¹, which led Blinowski and co-workers⁶ to propose a two-dimensional band structure. In the BR model the stage 1 GIC is treated as a collection of equivalent independent subsystems consisting of a graphene layer sandwiched between two intercalant layers. Electron transfer from the carbon atoms to the acceptor intercalant results in free holes in the graphene layer. The BR model makes use of a tight binding method, taking into account interactions between nearest neighbor carbon atoms. For the stage 1 compound the band structure corresponds to the 2D band structure of graphite¹² with the in-plane interactions between nearest neighbor carbon atoms taken into account only. In the vicinity of the Brillouin zone edge (K-point) the energy dispersion law becomes a linear function of the wave number k :

$$E_{c,v}(k) = \pm \frac{3}{2} \gamma_0 b k \quad (1).$$

Here γ_0 is a parameter which describes the carbon nearest-neighbor interaction energy, as defined by the resonance integral for the overlap of the wave functions at neighboring carbon atoms, and b ($= 1.42$ Å) is the carbon nearest-neighbor distance. The subscripts c and v label the conduction and valence bands, respectively. The Fermi energy is given by:

$$E_F = -\frac{3}{2}\gamma_0 b \left(\frac{S}{\pi}\right)^{1/2} \quad (2),$$

where $S = \pi k_F^2$ is the extremal Fermi surface cross-section, which in turn can be calculated from the measured frequency F of the SdH oscillation, $S = (2\pi e/\hbar)F$. The cyclotron effective mass is expressed in the Fermi energy as follows:

$$m^* = \frac{\hbar^2}{2\pi} \frac{\partial S}{\partial E} = \frac{4\hbar^2 E_F}{9\gamma_0^2 b^2} \quad (3).$$

The observation of a single fundamental frequency $F_1 = 1190$ T in the SdH signal of the stage 1 compound (Fig.1) is consistent with the BR model. With the experimental values of F_1 and m^* we have evaluated γ_0 by using eqs.(2)-(3) and obtain $\gamma_0 = 2.94$ eV. This value is in excellent agreement with the values $\gamma_0 \approx 2.8-3.0$ eV obtained for other acceptor GICs by reflectivity experiments². For pure graphite $\gamma_0 = 3.2$ eV (Ref.13). A reduction (in this case 9%) of the γ_0 -value in stage 1 acceptor-type GICs is expected, since the increase of carriers in the graphene layers results in a stronger screening of the atomic potential. The Fermi energy calculated by inserting $\gamma_0 = 2.94$ eV and the value for F_1 in eq.(2) amounts to -1.00 eV. The calculated band structure parameters are listed in Table I and the resulting band structure is shown in Fig.6. We conclude that the BR model gives a proper description of the band structure of the stage 1 PdAl₂Cl₈ GIC. The applicability of a pure 2D model is consistent with the measured $1/\cos\theta$ dependence of the fundamental frequency, indicating a perfect cylindrical Fermi surface and the high anisotropy ratio of the basal-plane and c-axis conductivity. The value $\sigma_a/\sigma_c \sim 10^6$ appears to be a prerequisite for pure 2D behavior. SdH data⁷ on the stage 1 compounds C_{9.3}AlCl_{3.4} and C₈H₂SO₄, with much lower anisotropy ratios of 10⁴ and 10⁵ (Ref. 11), respectively, could not be analysed satisfactorily within the 2D BR model. The charge transfer per carbon atom within this model is given by⁶ $f/l = 3\sqrt{3}b^2S/(4\pi^2)$ and amounts to the relatively small value of 0.030e in the stage 1 PdAl₂Cl₈ GIC.

B. Stage 2 compound

In order to calculate the band structure of the stage 2 GIC, Blinowski et al.⁶ treated the material as consisting of independent sets of two graphene layers bound by two intercalant layers. In the simplest approximation, only the nearest neighbor interactions in the graphite plane (γ_0) and the nearest neighbor interactions between carbon atoms in adjacent graphene layers (γ_1) are taken into account. The interlayer interaction partially removes the degeneracy of the valence and conduction bands at the K-point. The dispersion relations for the two valence bands are given by:

$$E_v^{1,2} = \frac{1}{2} \left(\pm \gamma_1 - \sqrt{\gamma_1^2 + 9\gamma_0^2 b^2 k^2} \right) \quad (4).$$

The Fermi energy is expressed as

$$E_F = \frac{1}{2} \left(\pm \gamma_1 - \sqrt{\gamma_1^2 + 9\gamma_0^2 b^2 \left(\frac{S_\pm}{\pi} \right)} \right) \quad (5),$$

where the plus (minus) sign is for the largest (smallest) extremal Fermi surface cross section, and the effective masses are given by:

$$m^* = \frac{2\hbar^2}{9\gamma_0^2 b^2} \left(\gamma_1^2 \pm \frac{9\gamma_0^2 b^2 S_\pm}{\pi} \right)^{1/2} \quad (6).$$

The BR model predicts the observation of one or two extremal Fermi surface cross sections, depending on whether $|E_F| < \gamma_1$ or $|E_F| > \gamma_1$. However, the Fourier spectrum of the stage 2 PdAl₂Cl₈ compound shows six frequencies (see inset in Fig.2 and Table I), which suggests that some frequencies must be attributed to higher harmonics and sum or difference frequencies. By comparing the values of the six frequencies listed in Table I we conclude that F_1 and F_3 are the relevant fundamental frequencies (these also give the largest peaks in the Fourier transform). F_4 and F_6 can be attributed to the 2nd and 3rd harmonics of F_1 , respectively.

Because the carrier concentration decreases with increasing stage number, the fundamental frequency $F_1=1190$ T of the stage 1 compound should be the highest. Therefore, $F_5(=1314$ T) cannot be a fundamental frequency. Instead, it can be attributed to the sum of the two fundamental frequencies F_1 and F_3 ($F_5=F_1+F_3$). When two subbands are occupied a complex SdH pattern is generated, and the highest frequency F_H may be modulated with the lower frequency F_L . Sum (F_H+F_L) and difference (F_H-F_L) frequencies arise due to elastic intersubband scattering. Apparently, for the stage 2 compound only the sum frequency is observable.

At the moment we do not have a truly satisfactory explanation for the frequency $F_2=495$ T. The proximity of F_1 and F_2 indicates splitting of a fundamental frequency. Such a splitting might be the result of a weakly undulating Fermi surface along the k_c direction, due to interactions between the sets of double graphene layers on either side of the intercalant layer. However, a study of the angular dependence of the SdH oscillations of the stage 2 compound did not give evidence for deviations from the 2D cylindrical Fermi surface. We could follow F_1 and F_2 up to 23° and 17° respectively. At these angles we did not observe any significant deviation from the $1/\cos\theta$ dependence. A second explanation for the splitting might be found in intercalant-layer density or chemical inhomogeneities. Density inhomogeneities could arise due to intercalant island formation, which would produce a perturbation in the graphene-graphene or graphene-intercalant interactions and hence affect the bandstructure. In other GICs such as those containing SbCl_5 , inhomogeneity within the intercalate layer is associated with different chemical species present within a same gallery. Experimental evidence for an inhomogeneous intercalant distribution was recently extracted from Raman scattering experiments¹⁴ on the PdAl_2Cl_8 GICs subjected to hydrostatic pressure. Also the presence of relatively broad peaks in the Fourier transform (see Fig.2) is not inconsistent with sample inhomogeneities. A two-fold and even four-fold splitting of frequencies due to intercalant islands has been reported for stage 3 SbCl_5 GIC⁹. The splitting was found to be time dependent, which is attributed to melting of different intercalant islands¹⁵. For the stage 2 PdAl_2Cl_8 GIC we did not observe any time dependence. Finally, we remark that it cannot be ruled out completely that the splitting is an artefact of the Fourier transform, as the difference F_2-F_1 depends on the field range used. This field-range dependence was not observed for the other frequency components.

Having made plausible that F_1 and F_3 are the fundamental frequencies, we calculate the relevant parameters of the energy spectrum ($|E_F|>\gamma_1$) within the BR model. In calculating the parameters, we furthermore assume that the interaction parameter between adjacent graphene layers γ_1 is not influenced by the intercalation process and is equal to the value for pure graphite ($\gamma=0.38$ eV). Inserting the values for S_{\pm} in eq.(5) (notice eq.(5) yields two equations with two unknown parameters) we calculate $\gamma_0=2.6$ eV and $E_F=-0.89$ eV (see Table I). The resulting band structure in the vicinity of the K-point is shown in Fig.6. The calculated value $\gamma_0=2.6$ eV is smaller than that determined for the stage 1 sample (2.94 eV). This cannot be understood on simple grounds, as we expect screening of the atomic potential to be less effective than in the stage 1 compound, which would imply a γ_0 -value in between the values for pure graphite and the stage 1 compound. This hints at a limited applicability of the BR model. On the other hand one cannot exclude a more complicated screening process. The cyclotron effective masses, calculated with the help of eq.(6), amount to $0.12m_0$ and $0.22m_0$ for the frequency components F_1 and F_3 , respectively. A comparison with experimental values cannot be made as data were only obtained at $T=4.2$ K. However, these values compare favorably to the experimental values obtained for the stage 1 and 3 compounds.

C. Stage 3 compound

The stage 3 compound can be treated as consisting of independent sets of three graphene layers bound by intercalant layers. A major difference with respect to the stage 2 compound is that electrostatic effects due to the excess charge in the graphene layers have to be taken into account. Different excess charge accumulates in the middle and outer graphene layers, and they are therefore no longer equivalent. This affects the electrostatic potential in the graphite subset and hence the band structure. In the BR model the difference in charge distribution in the middle and outer graphite layers is taken into account by an extra band parameter δ , which describes the resulting potential energy difference. For a stage 3 GIC there are 3 conduction and valence bands. The dispersion relations for the valence and the conduction bands in the vicinity of the K-point are:

$$\begin{aligned}
E_1^{c,v} &= \delta \pm |x| \\
E_2^{c,v} &= \pm \sqrt{\delta^2 + \gamma_1^2 + |x|^2 - \sqrt{\gamma_1^4 + (4\delta^2 + 2\gamma_1^2)|x|^2}} \\
E_3^{c,v} &= \pm \sqrt{\delta^2 + \gamma_1^2 + |x|^2 + \sqrt{\gamma_1^4 + (4\delta^2 + 2\gamma_1^2)|x|^2}}
\end{aligned} \tag{7}$$

where $|x|=(3/2)\gamma_0 b k$ as in eq.(1) and the plus (minus) sign applies for the conduction (valence) band. The extremal cross sections of the Fermi surfaces are given by:

$$\begin{aligned}
S_1 &= (E_F - \delta)^2 \frac{4\pi}{9\gamma_0^2 b^2} \\
S_2 &= (E_F^2 + \delta^2 + \sqrt{4E_F^2 \delta^2 + 2\gamma_1^2 (E_F^2 - \delta^2)}) \frac{4\pi}{9\gamma_0^2 b^2} \\
S_3 &= (E_F^2 + \delta^2 - \sqrt{4E_F^2 \delta^2 + 2\gamma_1^2 (E_F^2 - \delta^2)}) \frac{4\pi}{9\gamma_0^2 b^2}
\end{aligned} \tag{8}$$

In the BR model⁶ the number of observable SdH frequencies depends on the relative values of E_F , γ_1 and δ , but is three at the most. However, the Fourier transform (see the inset in Fig.3 and Table I) reveals the presence of at least 6 frequencies. Because of its large amplitude $F_4= 506$ T is beyond doubt a fundamental frequency, with $F_6= 1012$ T as its second harmonic. Inspecting the remaining values in Table I we conclude that the other two fundamental frequencies are $F_2= 138$ T and $F_5= 574$ T, while $F_1= F_5-F_4$ and $F_3= F_5-F_2$ are difference frequencies. At the moment we cannot offer a satisfactory explanation for the additional small peak in the Fourier transform at 771 T.

Accepting that the fundamental frequencies are F_2 , F_4 and F_5 , we next evaluate the interaction energies γ_0 and δ and the Fermi energy E_F using eq.8, where we take $\gamma_1= 0.38$ eV as for pure graphite. We calculate $\gamma_0= 1.3$ eV, $\delta= 0.15$ eV and $E_F= -0.62$ eV (see Table I). The calculated band structure is shown in Fig.6. The resulting value of γ_0 is much lower than the values found for the stage 1-2 compounds and pure graphite and therefore seems unrealistic. We conclude that the 2D BR model, although qualitatively correct, does not give an adequate description of the band structure of the stage 3 PdAl₂Cl₈ GIC.

One of the possible reasons for the inadequacy of the BR model is that the stage 3 PdAl₂Cl₈ GIC is indeed less 2D than the stage 1 and 2 GICs. In order to investigate this

possibility we have carried out angle dependent magnetoresistance experiments. Additional interactions along the c-axis result (for $B \parallel c$) in an undulating Fermi surface with two extremal cross sections located at $k_c=0$ (K-point) and $k_c=\pi/I_c$ (H-point). A plausible reason for an undulated Fermi surface is the presence of interactions between the graphite subsets across the intercalant layer. In this case the energy dispersion is expressed as follows¹⁶:

$$E_k = \delta - \frac{3}{2} \gamma_0 b (k_a + k_b) - 2t \cos(k_c I_c) \quad (9),$$

where t is the interlayer (along the c-direction) transfer integral. The in-plane dispersion is assumed to be isotropic. From this expression, the angular dependence of the cross section S of the weakly undulated Fermi surface is deduced¹⁶:

$$S = \frac{\left(\pi k_F^2 + \frac{4\pi m^* t}{\hbar^2} \cos(I_c k_c^0) J_0(I_c k_F \tan \theta) + O(t^2) \right)}{\cos \theta} \quad (10)$$

where k_F is the Fermi wave vector, I_c is the repeat distance, k_c^0 is the point in k-space where the cross sectional plane intersects the c-axis and $J_0(x)$ is the zero order Bessel function.

For the stage 3 GIC, we could follow the SdH oscillations up to $\theta=35^\circ$, with a better resolution than for the stage 1-2 compounds. The angular variation of the most pronounced fundamental frequency F_4 is plotted in Fig.5 (open circles). The dashed curve in Fig.5 describes the $1/\cos \theta$ dependence expected for a cylindrical Fermi surface. For $\theta > 15^\circ$ a significant deviation from the 2D behavior is observed. The data are well represented by the angular variation of the smallest circular cross-section of an undulating cylinder as given by eq. (10) (see solid line in Fig.5). The interlayer energy $t=5.6$ meV was used as a fit parameter. The smallest and largest circular cross-section frequencies at $\theta=0^\circ$ equal 506 T and 553 T, respectively, while the fundamental frequency of the uncorrugated Fermi surface equals 527 T. In fact, the latter value was used instead of F_4 in the analysis of the data within the BR model. The smallest circular cross-section frequency gives the strongest peak in the Fourier spectrum (see inset in Fig.3). A closer inspection of the Fourier spectrum shows that the largest circular cross-section frequency at 553 T is also observable, albeit as a very small peak

(not listed in Table I). We conclude that the stage 3 PdAl_2Cl_8 GIC is not strictly 2D. An undulating cylindrical Fermi surface was also reported for the stage 2 $\text{AlCl}_{3.4}$ GIC⁷, the heterointercalated stage 1 $\text{C}_{15}\text{CuCl}_2\cdot\text{ICl}_{1.2}$ GIC¹⁷ and for stage 1 CdCl_2 GIC¹⁸.

The amplitude of the SdH oscillations decreases rapidly with increasing angle θ between the magnetic field and the c-axis. This prevents a study of the angular dependence of the SdH signal over a wide range. In the literature, this rapid decrease is sometimes attributed to enhanced scattering of holes at the intercalant layer. The idea is that upon rotation of the sample the Lorentz force drives the carriers more and more to the intercalant layer. Below, we show that one does not need to evoke such a mechanism, as the angular dependence of the SdH amplitude is satisfactorily described by a model¹⁹ based on the general theory of quantum oscillations developed by Lifshitz and Kosevich²⁰. In the model the angular dependence of the SdH amplitude is determined by the electron dispersion law for graphite¹² and the broadening of the levels due to carrier collisions with impurities. No additional scattering is needed for $\theta\neq 0$. The broadening of the energy levels is related to the relaxation time τ by the Dingle temperature $T_D=\pi\hbar/(4\pi k_B)$. According to Ref.19 the normalised amplitude of the SdH oscillation is given by

$$\frac{\rho_{\perp}^{amp}(\theta)}{\rho_{\perp}^{amp}(0)} = \sqrt{\cos\theta} \exp\left[-(\alpha T + T_D)\left(\frac{1}{\cos\theta} - 1\right)\right] \quad (11),$$

where α is

$$\alpha = \frac{2\pi^2 ck_B |E_F - \gamma_1|}{e\hbar B \eta^2} \quad (12).$$

In eq.(12) c is the speed of light and $\eta=(\sqrt{3}\gamma b)/2\hbar$. In Fig.7 we compare the angular variation of the normalised amplitude of frequency F_4 of the stage 3 GIC with eq.(11). The only fit parameter is the Dingle temperature which amounts to $T_D=76\pm4$ K. The quantum mobility²¹ determined from the magnetoresistance yields a Dingle temperature $T_D=66\pm7$ K. The adequate description of the angular amplitude dependence of the amplitude of the SdH signal

with eq.(11) confirms that one does not need additional scattering mechanisms in order to describe the data for $\theta \neq 0$.

V. CONCLUSIONS

We have investigated the energy spectrum of stage 1-3 PdAl_2Cl_8 acceptor-type GICs by the Shubnikov-de Haas effect and compared the data with the 2D band structure model proposed by Blinowski and co-workers⁶. For the stage 1-2 compounds the experimental data are properly described by the BR model. For the stage 1 compound we observe one fundamental frequency and deduce a value of 2.94 eV for the intraplane carbon-carbon interaction parameter γ_0 . For the stage two GIC, we find six frequency components in the SdH signal, of which two are fundamentals. In this case, the Fermi energy is larger than the nearest carbon-carbon interlayer interaction parameter γ_1 , and $\gamma_0 = 2.60$ eV. The angular variation of the fundamental frequencies shows that the Fermi surface consists of 1 and 2 straight cylinders for the stage 1 and 2 compounds, respectively, providing clear evidence of their 2D nature.

For the stage 3 compound the SdH data show the presence of at least 6 frequency components. We argue that three of these are fundamental frequencies in agreement with the BR model. However, the analysis results in an unrealistic value $\gamma_0 = 1.3$ eV, which strongly suggests that this 2D model does not yield a proper description. This we attribute to additional interactions between the graphite subsets across the intercalant layer. Deviations from the 2D behavior are confirmed by measuring the angular variation of one of the fundamental frequencies. The corresponding Fermi surface is a weakly undulating cylinder and the additional interaction energy parameter t equals 5.6 meV. Finally we show that the angular dependence of the amplitude of the SdH signal is completely described by the standard Lifshitz-Kosevich formalism.

Acknowledgements

This work was part of the research program of the Dutch "Stichting FOM" (Foundation for Fundamental Research of Matter). The authors thank V.A. Kulbachinskii for helpful discussions.

References

¹ *Semimetals - I. Graphite and its compounds*, N.B. Brandt, S.M. Chudinov, and Ya.G. Ponomarev (North Holland, Amsterdam, 1988) [Modern Problems in Condensed Matter Sciences **20.1**]

² *Graphite Intercalation Compounds II*, eds. H. Zabel and S.A. Solin (Springer Verlag, Berlin, 1992) [Springer Series in Material Science **18**]

³ M.S. Dresselhaus and G. Dresselhaus, *Adv. Phys.* **30**, 139 (1981)

⁴ V. Polo, M. Lelaurain, R. Vangelisti, and E. McRae, *Mol. Cryst. Liq. Cryst.* **245**, 75 (1994)

⁵ G.M.T. Foley, C. Zeller, E.R. Falardeau, and F.L. Vogel, *Solid State Comm.* **24**, 371 (1977)

⁶ J. Blinowski, Nguyen Hy Hau, C. Rigaux, J.P. Vieren, R. Le Toullec, G. Furdin, A. Hérold, and J. Melin, *J. Physique* **41**, 47 (1980); J. Blinowski and C. Rigaux, *J. Physique* **41**, 667 (1980)

⁷ V.A. Kulbachinskii, S.G. Ionov, S.A. Lapin, and A. de Visser, *Phys. Rev. B* **51**, 10313 (1995)

⁸ D. Marchesan, J.D. Palidwar, P.K. Ummat, and W.R. Datars, *J. Phys.: Condens. Matter* **8**, 991 (1996); W.R. Datars, J.D. Palidwar, T.R. Chien, P.K. Ummat, H. Aoki, and S. Uji, *Phys. Rev. B* **53**, 1579 (1996)

⁹ H. Zaleski, P.K. Ummat, and W.R. Datars, *J. Phys. C: Solid State Phys.* **17**, 3167 (1984); H. Zaleski, P.K. Ummat, and W.R. Datars, *Phys. Rev. B* **35**, 2958 (1987); G. Wang, H. Zaleski, P.K. Ummat, and W.R. Datars, *Phys. Rev. B* **37**, 9029 (1988)

¹⁰ V. Polo and R. Vangelisti, *Ann. Chim. Fr.* **19**, 177 (1994)

¹¹ E. McRae and J.F. Marêché, *J. Mater. Res.* **3**, 75 (1988)

¹² J.C. Slonczewski and P.R. Weiss, *Phys. Rev.* **109**, 272 (1958)

¹³ E. Mendez, A. Misu, and M.S. Dresselhaus, *Phys. Rev. B* **21**, 287 (1980)

¹⁴ E. McRae et al., unpublished

¹⁵ D.M. Hwang and G. Nicolaides, *Solid State Comm.* **49**, 483 (1984)

¹⁶ K. Yamaji, *J. Phys. Soc. Jpn.* **58**, 1520 (1989)

¹⁷ V.V. Avdeev, V.Ya. Akim, N.B. Brandt, V.N. Davydov, V.A. Kulbachinskii, and S.G. Ionov, *Sov. Phys. JETP* **67**, 2496 (1989)

¹⁸ W.R. Datars, P.K. Ummat, H. Aoki, and S. Uji, *Phys. Rev. B* **48**, 18174 (1993)

¹⁹ N.B. Brandt, V.N. Davydov, V.A. Kulbachinskii, and O.M. Nikitina, Sov. Phys. Solid State **29**, 1014 (1987)

²⁰ I.M. Lifshitz and A.M. Kosevich, Sov. Phys. JETP **11**, 637 (1960); For a review on quantum oscillatory phenomena see: *Magnetic oscillations in metals*, D. Shoenberg (Cambridge University Press, Cambridge, 1984)

²¹ S. Yamada, J. Appl. Phys. **72**, 569 (1992)

Table and Table Captions

Table I: Experimentally determined Shubnikov-de Haas frequencies, F , carrier densities n_{SdH} , and cyclotron effective masses, m^*/m_0 , for stage 1-3 PdAl_2Cl_8 GICs. Values for the Fermi energy E_F and the interaction parameters γ_0 have been calculated within the Blinowski-Rigaux model⁶. For the stage 2 and 3 compounds the peak numbers correspond to the labels in Figs.2 and 3.

Stage number	Peak number	F (T)	n_{SdH} (m^{-3})	m^*/m_0	E_F (eV)	γ_0 (eV)
1	1	1190 ± 2	1.20×10^{27}	0.25	-1.00	2.94
2	1	462 ± 3	3.66×10^{26}	-	-0.89	2.60
	2	495 ± 20	-	-		
	3	848 ± 7	6.59×10^{26}	-		
	4	895 ± 10	-	-		
	5	1314 ± 4	-	-		
	6	1396 ± 4	-	-		
3	1	69 ± 2	-	-	-0.62	1.3
	2	138 ± 2	8.11×10^{25}	0.20		
	3	439 ± 7	-	-		
	4	506 ± 6	3.14×10^{26}	0.28		
	5	574 ± 3	3.41×10^{26}	-		
	6	1012 ± 10	-	-		

Figure captions

Fig.1 Magnetoresistance of the stage 1 PdAl_2Cl_8 graphite intercalation compound at $T= 4.2$ K. The inset shows the Fourier spectrum of the SdH oscillations.

Fig.2 Magnetoresistance of the stage 2 PdAl_2Cl_8 GIC at $T= 4.2$ K. The inset shows the Fourier spectrum of the SdH oscillations.

Fig.3 Magnetoresistance of the stage 3 PdAl_2Cl_8 GIC at $T= 1.5$ K. The inset shows the Fourier spectrum of the SdH oscillations.

Fig.4 Magnetoresistance of the stage 3 PdAl_2Cl_8 GIC measured at angles θ of 0° , 18° and 32° . The data at 18° and 32° are shifted upwards by $5 \text{ m}\Omega$ and $10 \text{ m}\Omega$, respectively. Data are taken at $T= 4.2$ K.

Fig.5 Angular dependence of the fundamental frequency F_4 of the stage 3 PdAl_2Cl_8 GIC measured at $T= 4.2$ K. The open circles are the data points. The data follow the solid line, which gives the angular dependence of the minimal circular cross-section frequency of an undulating cylindrical Fermi surface. The dashed line gives the 2D $1/\cos\theta$ dependence for a straight cylindrical Fermi surface.

Fig.6 Band structure near the Brillouin zone edge (K-point) for stage 1-3 PdAl_2Cl_8 acceptor-GIC. Valence and conduction bands are denoted by v and c respectively. The Fermi energy E_F and the interaction parameter γ_0 have been determined from SdH data. For the stage 1-3 compounds γ_0 determines the slopes of the energy bands (at high k -values). For the stage 2 compound γ_1 determines the distance in energy between the valence and conduction bands. For the stage 3 compound the additional interaction energy δ results in an upward shift of the energy bands.

Fig.7 Angular dependence of the relative change of the amplitude for the stage 3 PdAl_2Cl_8 GIC. The dashed curve represents a fit to eq.(11) with a Dingle temperature $T_D= 76$ K.

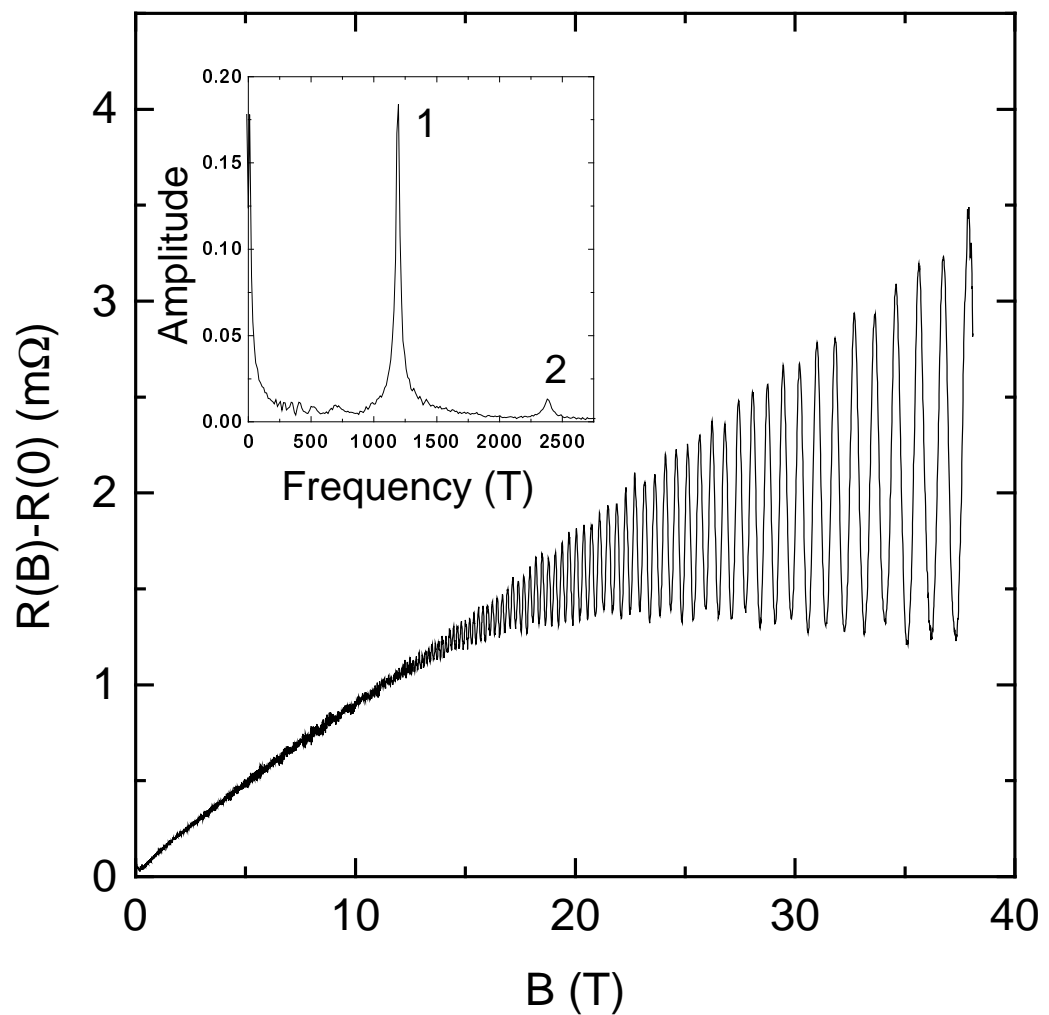


Figure 1

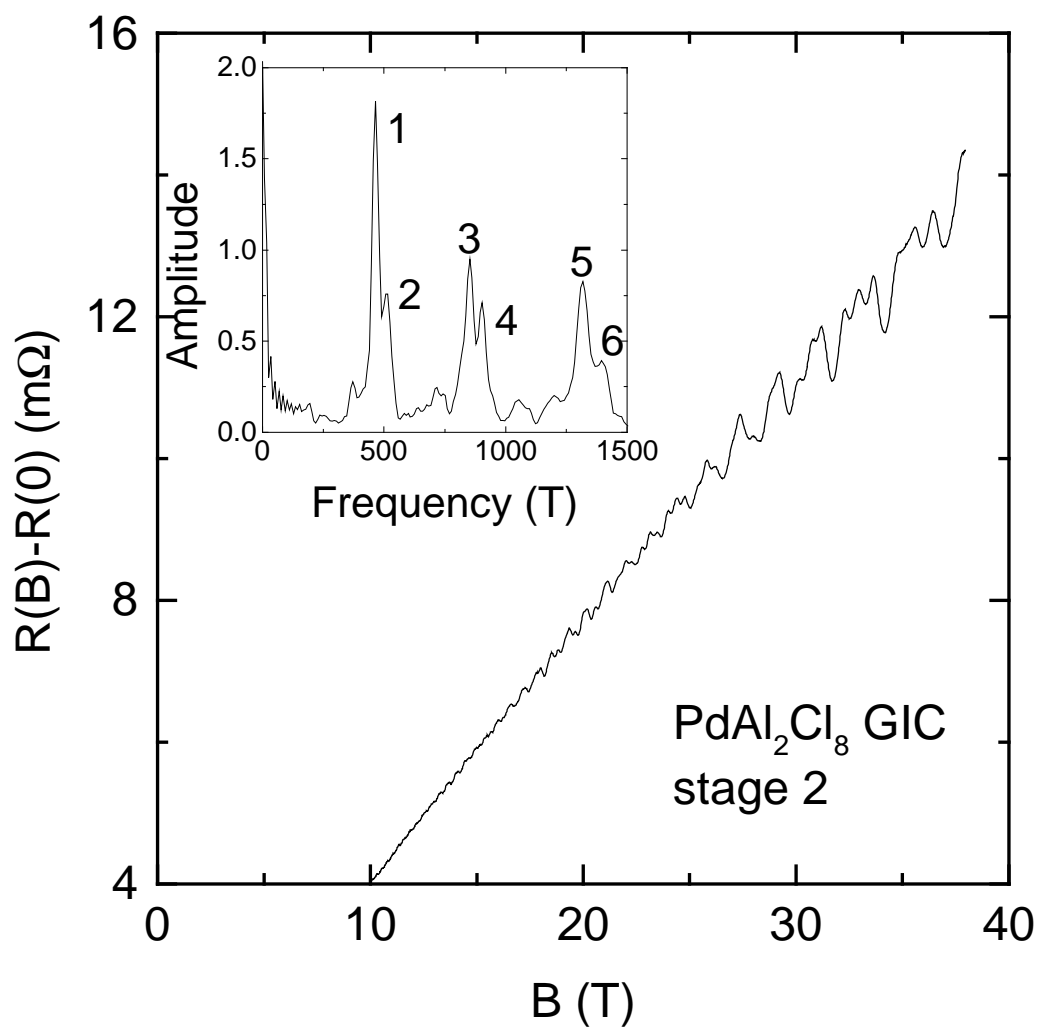


Figure 2

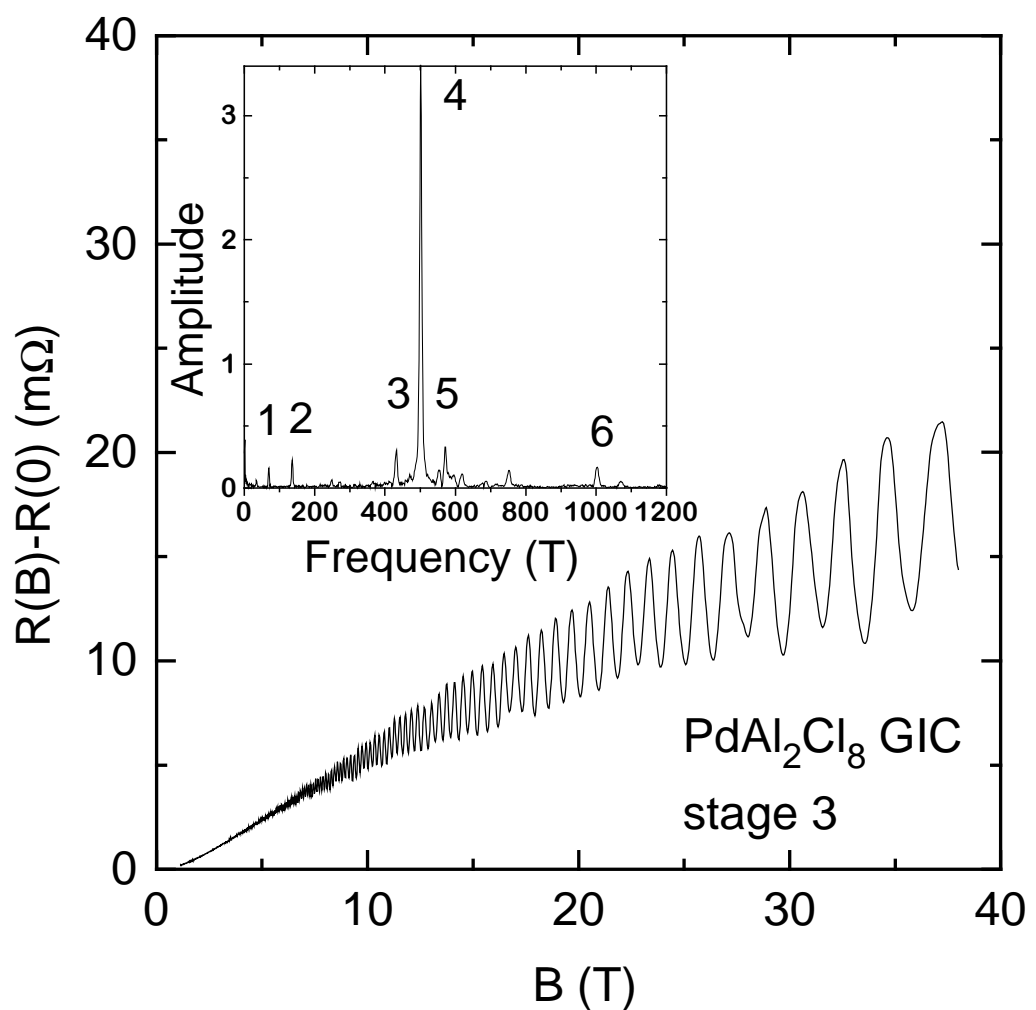


Figure 3

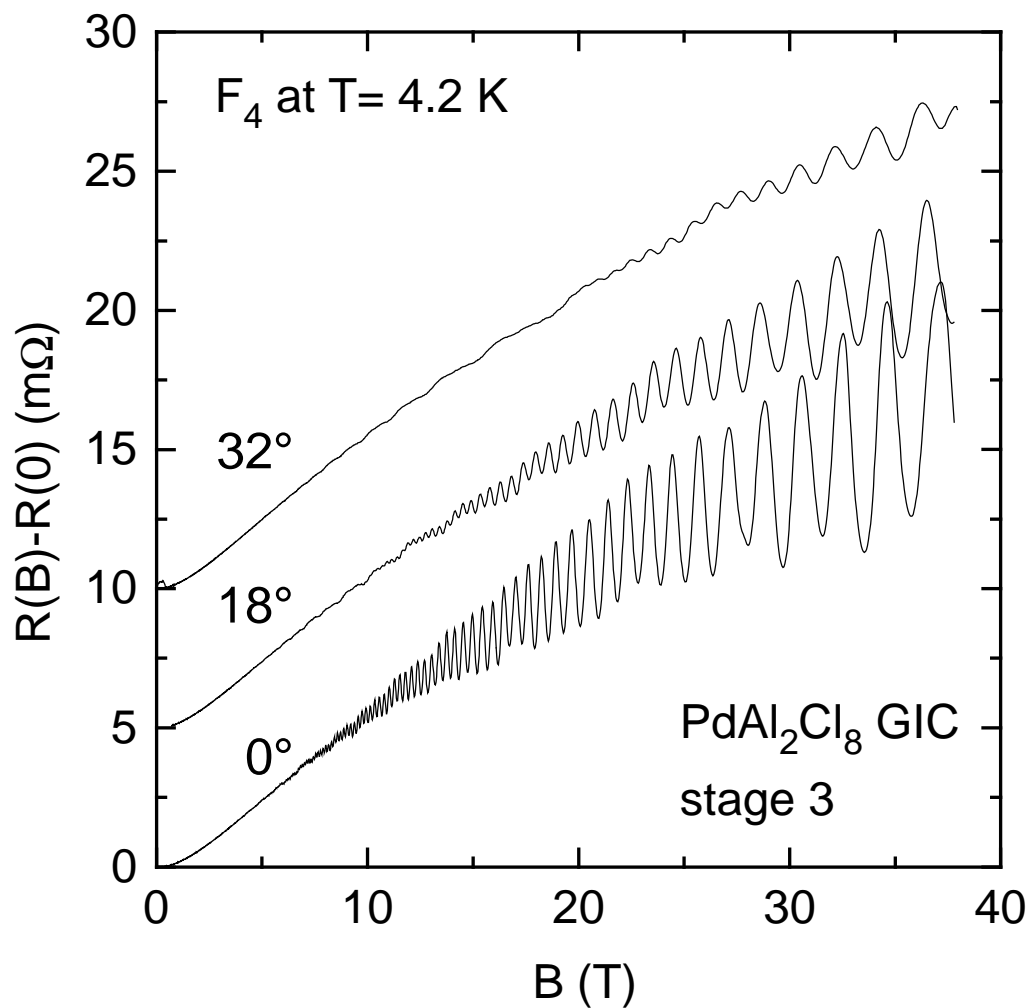


Figure 4

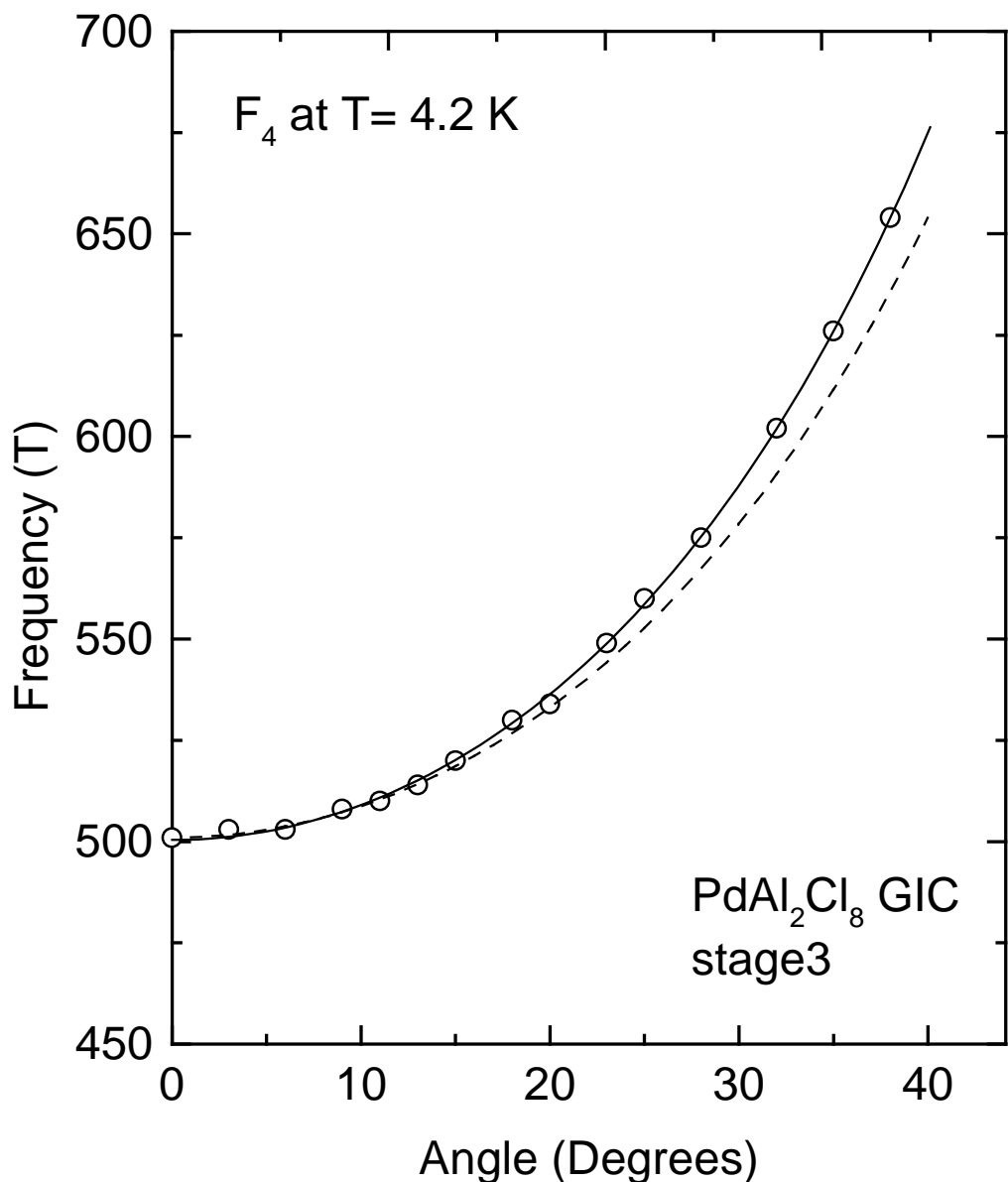


Figure 5

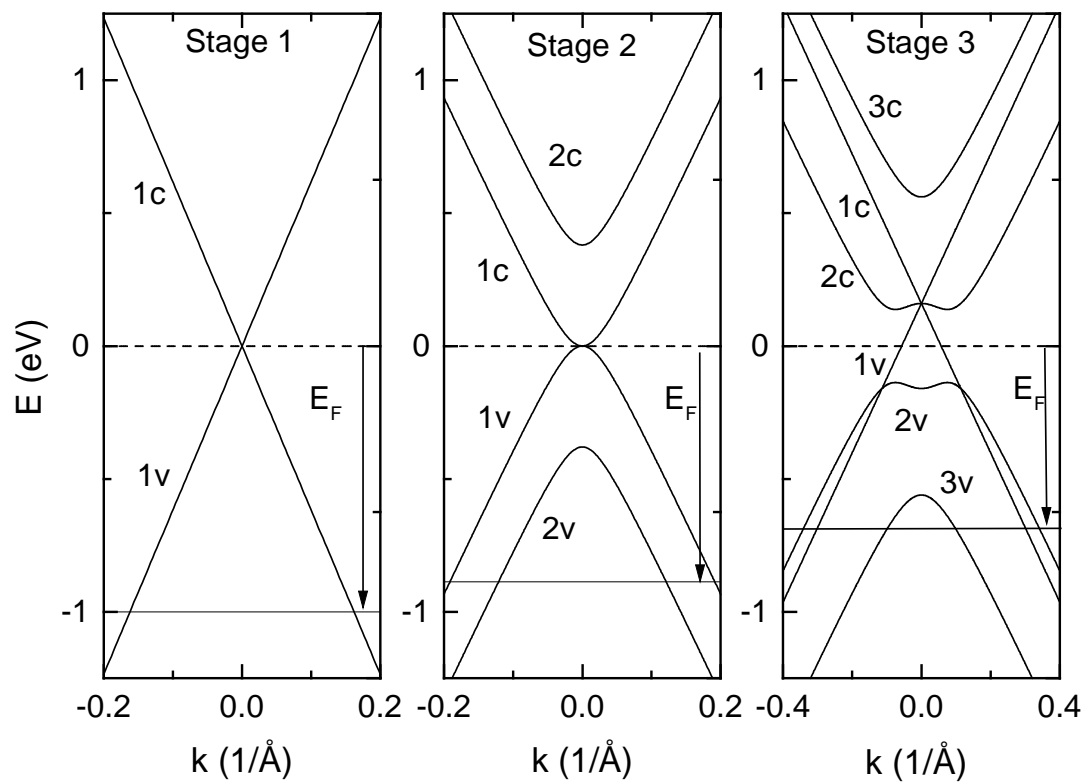


Figure 6

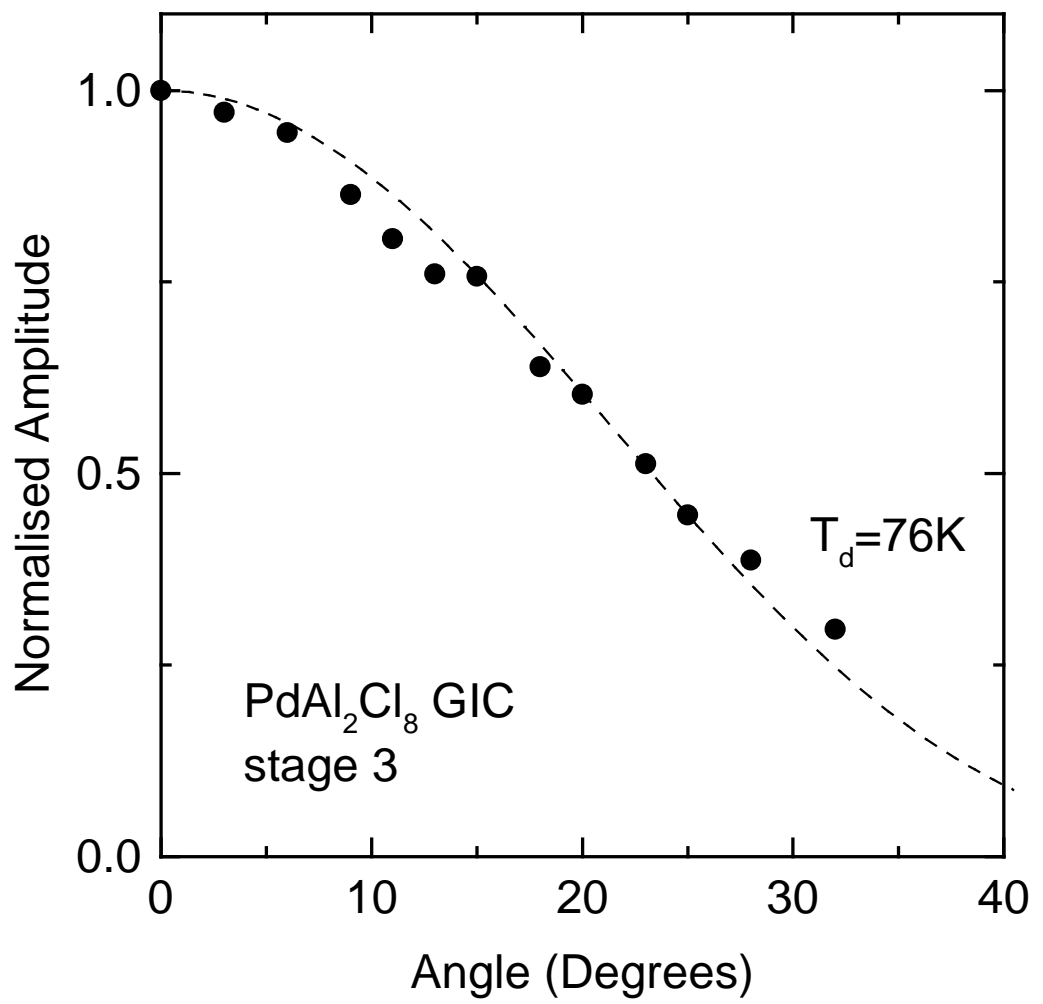


Figure 7